

On Plastic Zones and Fracture Strengths in Some Metal Matrix Composites

J.F. Zarzour and A.J. Paul

Based on a Dugdale-type approach for cancelling the singularity at the crack tip, an attempt was made to predict the overall stress distributions, as well as the size of the plastic zone found in notched metal matrix composite plate. The work was developed by considering notched, unidirectionally reinforced fibrous metal matrix composite plate under uniform normal tension load. Predictions of the proposed method were compared with the experimental results, and a fairly good agreement was observed. Simple closed form expressions for the local stresses and fracture strength are provided.

1. Introduction

EXPERIMENTAL observations of notched metal matrix composite plate have revealed the existence of matrix yielding between fibers and in locations remote from the notch tip. Details of these observations are discussed by Awerbuch and Hahn,[1] Reedy,[2,3] Poe and Sova,[4] and Dvorak and Bahei-El-Din.[5] These plastic deformations, which take place at loads well below the fracture load, are described as discrete plastic shear bands with length scales that exceed the length of the notch by several orders of magnitude. The presence of this large-scale plasticity produces notch-tip blunting and gives rise to stress redistribution ahead of the notch tip. Therefore, for a sound understanding of the strength of these composites, it is important to obtain an accurate evaluation of the length of these zones, as well as the local stress fields ahead of the notch tip.

Awerbuch and Hahn[1] characterized the matrix damage by longitudinal shear band deformation. Similarly, the experimental results of Dvorak and Bahei-El-Din,[5] using the bar code technique, for center-notched B/Al composites (Fig. 1), have indicated the existence of plastic zone deformations that are 3 to 17 times the length of the original notch and about 0.2 mm wide (Fig. 2). Most of the existing methods for determining these zones relied on the application of the J-integral and finite-element analysis. Such methods were developed and discussed by Rice,[7] McClintock,[8] Tirosh,[9] and recently by Bahei- El-Din *et al.*[10] Others have used dislocation models to represent the plastic zone, mainly Bibly and Swinden,[11] Riedel,[12] Vitek,[13] and Kujawski and Ellyin.[14] Unlike these computational methods where the solution is rather "expensive," the present work presents a simple numerical scheme for obtaining the length of these zones.

2. Numerical Model

The strip yield model, developed by Dugdale,[15] provides the solution for the dimensions of the localized plastic zone at a crack tip. In this model, the effective crack length is longer than the physical length, and the additional crack increment is considered to be at yield. Consequently, a stress singularity cannot exist at the notional crack tip, because at that point the stress cannot exceed the yield strength of an elastic-perfectly plastic material. Accordingly, the present analysis models the plastic zones as vertical cracks loaded by the composite flow stress in shear τ^*, which was confirmed by Bahei-El-Din *et al.*[10] using finite-element analysis to be the only significant stress compo-

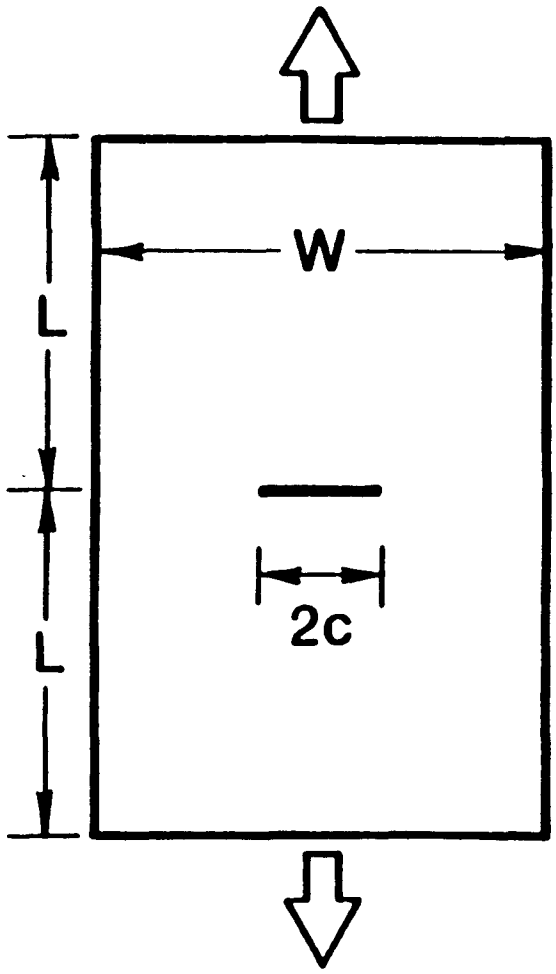

Fig. 1 Geometry of center-notched specimens under uniform normal load.

J.F. Zarzour and **A.J. Paul**, Concurrent Technologies Corporation, Johnstown, Pennsylvania.

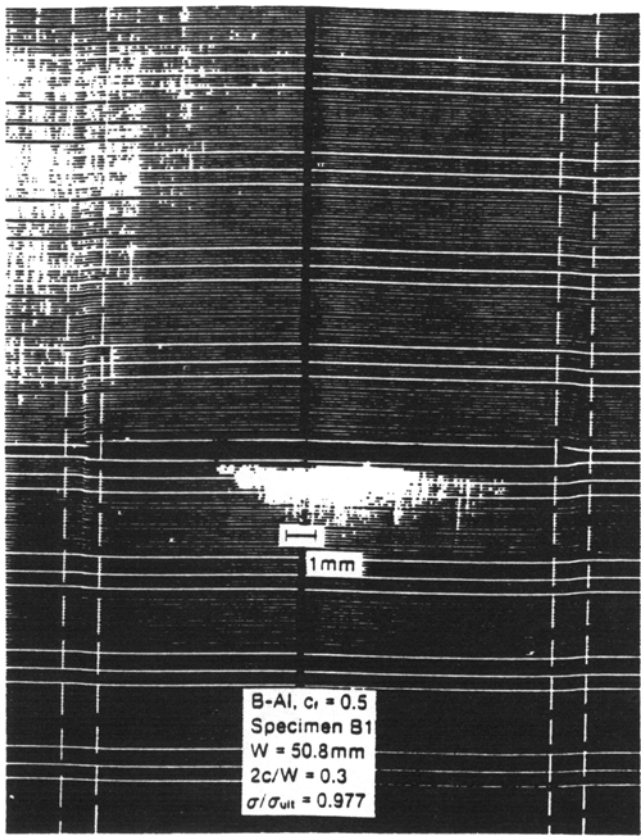

Fig. 2 Discrete plastic zones at the notch tip found by the bar code technique.[6]

nent in the plastic zone. Therefore, the two vertical cracks, together with the original notch, form an H-crack configuration loaded remotely by a uniform axial tension, P^0, and locally by the composite flow stress in shear, τ^* (see Fig. 3). Following the principle of superposition, the configuration of Fig. 3 can be decomposed into two configurations, as shown in Fig. 3(a) and Fig. 3(b), respectively. It follows that the effective mode II stress-intensity factor at each tip of the H-crack, $K_{II}(A)$, can be obtained as the sum of $K_{II}(A)$ from each configuration:

$$K_{II}(A)(R/c, P^0/\tau^*) = K_{II}(A)(R/c, P^0) + K_{II}(A)(R/c, \tau^*) \quad [1]$$

where R/c is the ratio of the plastic zone height to the half crack length. The length of the plastic zone, R, is then obtained with the condition that $K_{II}(A)(R/c, P^0/\tau^*)$ must vanish at each tip of the H-crack configuration. At the onset of fracture, the axial load, P^0, the composite flow stress in shear, τ^*, and the notch length, $2c$, are known. Thus, the value of R for which Eq 1 is satisfied represents the actual plastic zone height. An example that illustrates the calculation of R for the case of $(P^0/\tau^*) = 1$ and $c = 1$ for the B/Al composite is shown in Fig. 4. In actual calculations, the K_{II} values were obtained at several R values. However, the plastic zone length R for which K_{II} was equal to zero was found by interpolation. Because a closed form solution for K_{II} is not available in the literature, a numerical scheme for crack analysis proposed by Benveniste *et al.*[16] was used. Material properties for the two metal matrix composite systems considered herein—B/Al and Fp/Al—are shown in Table 1.

For the center-notched B/Al composite, Table 2 shows the corresponding results for R, predicted by the present model, as well as those found by Bahei-El-Din *et al.*[10] using the finite-

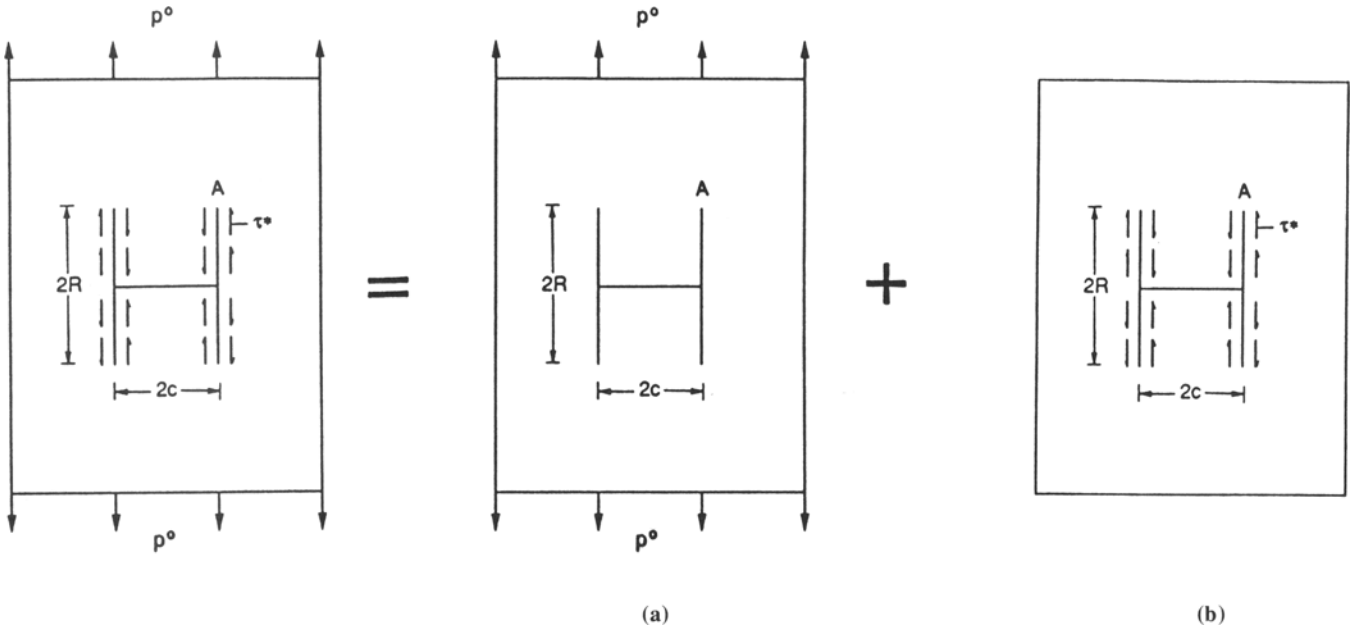

Fig. 3 Superposition of the H-crack under remote uniform axial tension, P^0, and local piecewise uniform shear, τ^*, into (**a**) H-crack loaded only by the remote uniform axial tension, P^0; (**b**) H-crack loaded only by the local piecewise uniform shear, τ^*.

Table 1 Elastic Constants of 6061 Al (F), Boron (B/Al), and Al_2O_3 (FP/Al)

Material	E_A, GPa	E_T, GPa	G_A, GPa	G_T, GPa	ν_A	Composite flow stress, τ^*, MPa	Fiber diameter, (d), mm	Unnotched strength, σ_{un}(min)/σ_{un}(max), MPa	Reference
6061 Al	72.5	72.5	27.3	27.3	0.33	...	...	...	...
Boron	400.0	400.0	166.7	166.7	0.20	...	...	...	...
6061 Al/B (c_f = 0.5)	235.6	144.8	...	...	...	...	...	...	Experimental (Ref 6)
	237.3	143.1	55.1	...	0.21	96	0.142	1685-1710	Experimental (Ref 4)
	237.0	158.7	67.4	59.2	0.25	...	...	...	Self-consistent estimates
Alumina	379	379	157.5	...	0.203	...	...	...	...
FP/Al (c_f = 0.35)	167.08	114.7	44.2	...	0.279	115	0.02	482-580	Experimental (Ref 24)

Table 2 Comparison of Current Predictions of Discrete Plastic Zone Lengths (R) with Finite-Element Results

Specimen No.	Specimen dimensions W, mm	$2c$, mm	$2c/W$	P_{ul}, MPa	Plastic zone length (R), mm R(a)	R(b)	R(c)
1	19.1	0.5	0.026	1365	4.3	3.7	3.55
2	19.1	0.5	0.026	1371	4.3	3.7	3.57
3	19.1	1.3	0.068	1124	8.1	6.5	7.61
4	19.1	1.3	0.068	1165	8.1	6.5	7.88
5	50.8	2.5	0.050	929	10.0	9.77	12.0
6	50.8	2.5	0.050	1051	12.5	11.5	13.6
7	50.8	5.1	0.1	921	25.0	21.0	24.4
8	50.8	5.1	0.1	934	25.0	22.0	24.8
9	50.8	15.2	0.3	665	52.5	50.7	52.6
10	50.8	15.2	0.3	666	52.5	50.7	52.7
11	50.8	15.2	0.3	701	55.0	52.0	55.5
12	50.8	15.2	0.3	645	50.0	49.5	51.1
13	50.8	25.4	0.5	534	72.5	73.5	70.6
14	50.8	25.4	0.5	502	67.5	69.0	66.4
15	101.6	5.1	0.05	969	25.0	21.0	25.7
16	101.6	10.2	0.1	790	42.5	41.0	42.0
17	101.6	10.2	0.1	775	40.0	40.0	41.0
18	101.6	30.5	0.3	541	80.0	80.5	86
19	101.6	30.5	0.3	506	77.5	77.0	80.3
20	101.6	30.5	0.3	470	75.0	74.0	74.6
21	101.6	50.8	0.5	393	85.0	90.0	103
22	101.6	50.8	0.5	382	85.0	90.0	101

(a) Predicted by Bahei-El-Din *et al.*[10] (b) Present predictions. (c) Predicted by the equilibrium equation: $R = cP_{ul}/\tau^*$.

element method. Fairly good agreement is obtained even when the notch and the free edges of the specimen are in close proximity. Other interesting features of the results show that the plastic zone length/half-notch length ratio, R/c, is inversely proportional to the notch aspect ratio, $2c/W$.

3. Fracture Initiation—Strength Prediction

As described earlier in this work, the presence of long discrete plastic zones causes notch-tip blunting and local stress redistribution. Thus, it is believed that models that account for the detailed phenomena at a crack tip do represent a more realistic approach to fracture of the present problem. The idea of average stress technique, proposed by Nuismer and Whitney[17] and Dvorak *et al.*[6] is adopted here with some simplifications. The current model is postulated in the following way: The onset of fracture is controlled by the average normal stress over a material representative volume element $\bar{\omega}$ in the vicinity of the notch tip; fracture will occur when the value of this average becomes

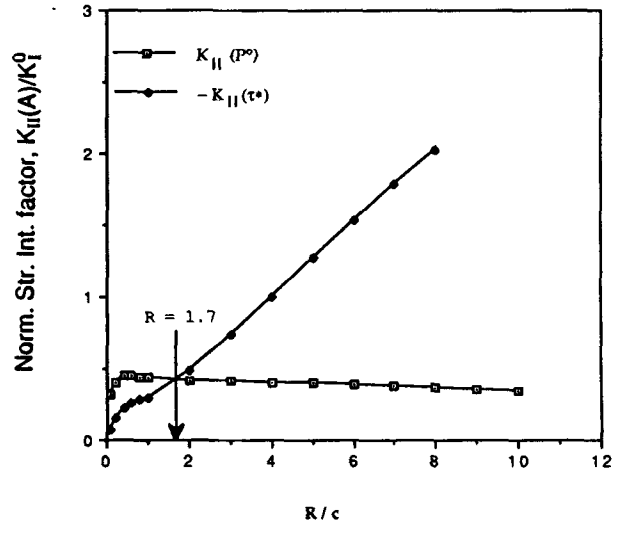

Fig. 4 Evaluation of the plastic zone height, R, according to the Dugdale's model ($K_I^0 = P^0\sqrt{\pi c}$).

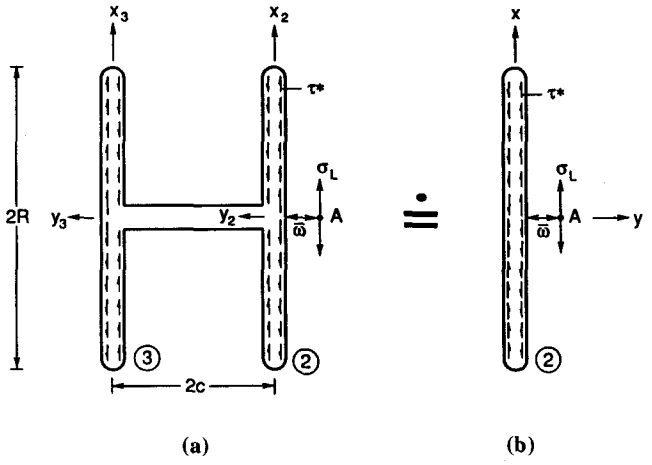

Fig. 5 Modeling of the notch and the plastic zones by an *H*-crack configuration (**a**) and approximation of the *H*-crack by a single vertical crack loaded by the composite flow stress, τ^* (**b**).

equal to a critical value, such as the unnotched strength of the material. Following the evaluation of the length of the plastic zones, the local normal stress field generated ahead of the blunted notch tip can be determined. Suppose that the zone length R for a certain specimen has been determined and one is now interested in finding the corresponding normal stress σ_L ahead of the notch (see Fig. 5b). By superposition, the total normal stress σ_L can be decomposed into two parts: σ_{lig} and σ_{pl}, as shown in Fig. 6(a) and Fig. 6(c), respectively. In this case, σ_{lig} denotes a uniform ligament stress, which is simply a function of the applied load and the geometry of the specimen:

$$\sigma_{lig} = P^0 / \left(1 - \frac{2c}{W}\right) \qquad [2]$$

where $2c$ is the length of the notch, W is the width of the specimen, and P^0 is the applied tension load. σ_{pl}, which has zero average stress over the ligament (from equilibrium considerations), depends primarily on the length of the zone as well as the geometry of the specimen. Ideally, σ_{pl} can be obtained with respect to the entire *H*-crack configuration, as shown in Fig. 6(c). However, due to the stress shielding effect of the large plastic zone over the adjacent small distance $\bar{\omega}$, the present calculations of σ_{pl} are approximated based on the solution of a single crack of length $2R$, loaded by a piecewise uniform shear flow stress τ^* (see Fig. 5b). According to the exact solution of stress fields generated by a single crack under point-load conditions, in an infinite orthotropic medium,[18] the case of point-concentrated loads in shear Q, as shown in Fig. A-1 of the Appendix, admits the following stress potential functions:

$$\Phi(z_1) = \frac{1}{(s_2 - s_1)} \frac{Q}{(z_1 - s)} \left[\frac{R^2 - s^2}{z_1^2 - R^2}\right]^{1/2}$$

$$\Psi(z_2) = \frac{1}{(s_1 - s_2)} \frac{Q}{(z_2 - s)} \left[\frac{R^2 - s^2}{z_2^2 - s^2}\right]^{1/2}$$

where s_1 and s_2 are the roots of the characteristic equation (see Ref 15), and s is the distance between the position of the applied load and the origin of the local reference frame of the crack. The z_1 and z_2 quantities are two complex variables given by:

$$z_1 = x + s_1 y$$

$$z_2 = x + s_2 y \qquad [3]$$

Therefore, the expression of the normal stress component σ_{pl} can be written as:

$$\sigma_{pl} = 2Re[s_1^2 \Phi(z_1) + s_2^2 \Psi(z_2)] \qquad [4]$$

and, according to Fig. 5(b), the integration of the point loads solution along the crack length is given by:

$$(s_2 - s_1)\Phi(z_1) = \frac{Q}{2\pi(z_1^2 - R^2)^{1/2}} \left\{ \int_{-R}^{0} \frac{(R^2 - s^2)^{1/2}}{z_1 - s} ds - \int_{0}^{R} \frac{(R^2 - s^2)^{1/2}}{z_1 - s} ds \right\}$$

$$(s_1 - s_2)\Psi(z_2) = \frac{Q}{2\pi(z_2^2 - R^2)^{1/2}} \left\{ \int_{-R}^{0} \frac{(R^2 - s^2)^{1/2}}{z_2 - s} ds - \int_{0}^{R} \frac{(R^2 - s^2)^{1/2}}{z_2 - s} ds \right\} \qquad [5]$$

Identifying $Q = \tau^*$ and substituting the solution of Eq 5 into Eq 4, one finds the final form of the normal stress field as (for explicit derivations, see the Appendix):

$$\sigma_{pl}(x,y)/\tau^* = Re\left\{ \frac{s_1^2}{\pi(s_2 - s_1)} \left[\left(\frac{2}{(z_1/R)^2 - 1} \right)^{1/2} + i \ln(\alpha_1) \right] + \frac{s_2^2}{\pi(s_1 - s_2)} \left[\left(\frac{2}{(z_2/R)^2 - 1} \right)^{1/2} + i \ln(\alpha_2) \right] \right\} \qquad [6]$$

where

$$\alpha_{1,2} = \frac{(z_{1,2}/R)^2 + 2i\left[\left(z_{1,2}/R\right)^2 - 1\right]^{1/2} - 2}{(z_{1,2}/R)^2}$$

Because the stress of interest is the normal component acting ahead of the notch tip, over a distance $\bar{\omega}$, $(x = 0)$, as shown in Fig. 5(b). Therefore, Eq 6 can be greatly simplified. The complex variables z_1 and z_2 now have the form:

$$z_1 = s_1 y$$

$$z_2 = s_2 y$$

In addition, for a unidirectional composite system, the material principal axes coincide with the Cartesian axes, and the roots s_1 and s_2 are purely imaginary:[19]

$$z_1 = ia_1 y$$

$$z_2 = ia_2 y$$

where a_1 and a_2 denote the imaginary parts of s_1 and s_2, respectively. With these simplifications, the solution of Eq 6 can be reduced to the following form:

$$\sigma_{pl}(0,y)/\tau^* = \frac{2}{\pi(a_2 - a_1)}\left\{a_1^2\left[\frac{1}{(1 + a_1^2(y/R)^2)^{1/2}} - \ln(\alpha_1)\right] + a_2^2\left[\frac{1}{(1 + a_2^2(y/R)^2)^{1/2}} + \ln(\alpha_2)\right]\right\} \quad [7]$$

where

$$\alpha_{1,2} = \frac{1 + [1 + a_{1,2}^2(y/R)^2]^{1/2}}{a_{1,2}(y/R)}$$

Note that as y approaches zero in Eq 7, σ_{pl} exhibits a logarithmic singularity.

Finally, the overall normal stress component ($\sigma_L = \sigma_{lig} + \sigma_{pl}$) ahead of the notch tip ($x = 0$) can now be written as:

$$\sigma_L = P^0/\left(1 - \frac{2c}{W}\right) + 2\tau^*/\pi(a_2 - a_1)\left\{a_1^2\left[\frac{1}{(1 + a_1^2(y/R)^2)^{1/2}} - \ln(\alpha_1)\right] + a_2^2\left[\frac{-1}{(1 + a_2^2(y/R)^2)^{1/2}} + \ln(\alpha_2)\right]\right\} \quad [8]$$

The next step in the analysis is to provide an average of Eq 8 in the crack local reference system (along the y-axis), over a small distance $\bar{\omega}$ from the crack midlength, as shown in Fig. 5(b). The corresponding average stress field is (see Appendix for detailed derivations):

$$\bar{\sigma}_L/\tau^* = P^0/\left(1 - \frac{2c}{W}\right) + 2\tau^*/\pi(a_2 - a_1)\left\{-a_1^2 \ln\left[\frac{1 + (1 + (a_1/t)^2)^{1/2}}{(a_1/t)}\right] + a_2^2 \ln\left[\frac{1 + (1 + (a_2/t)^2)^{1/2}}{(a_2/t)}\right]\right\} \quad [9]$$

where $t = R/\bar{\omega}$.

The choice of a material representative volume element (RVE) depends primarily on the material system in question. In the literature, there are many ways to choose a representative volume element. Herein, a unit cell in a periodic hexagonal array model of the B/Al composite system is selected (see Ref 10). Figure 7 shows a transverse plane geometry of such a cell. Accordingly, the width $\bar{\omega}$ can be determined as:

$$\bar{\omega} = 2b = d(2\pi/3\sqrt{3}c_f)^{1/2} \quad [10]$$

where d is the fiber diameter and c_f is the fiber volume fraction. In the present analysis, $d = 0.142$ mm and $c_f = 0.5$; hence, $\bar{\omega} = 1.555\,d = 0.22$ mm. This length represents the dimension of the representative volume element in the y-direction; the specimen thickness is the other dimension. No other dimension was specified in the z-direction.

In accordance with the fracture criterion stated earlier in this work, fracture is presumed to take place once the average of normal stress components over a representative volume element reaches the unnotched strength of the material. At that moment, the applied normal load coincides with the ultimate load-bearing capacity ($P^0 = P_{ul}$). The corresponding criterion can be written in the following form:

$$P_{ul}/\left(1 - \frac{2c}{W}\right) + 2\tau^*/\pi(a_2 - a_1)\left[-a_1^2 \ln\left(\frac{1 + \sqrt{1 + a_1^2\beta^2}}{a_1\beta}\right) + a_2^2 \ln\left(\frac{1 + \sqrt{1 + a_2^2\beta^2}}{a_2\beta}\right)\right] - \sigma_{un} = 0 \quad [11]$$

where σ_{un} is the unnotched strength, and $\beta = \bar{\omega}/R$.

The use of Eq 11 necessitates an estimate of R, which was obtained numerically in the previous section. However, as indicated by Fig. 8, the computed results of the ratio of the plastic zone length to half crack length versus the ratio of overall stress to plastic zone shear stress at failure loads fall on a straight line. This linear relationship suggests that the plastic zone length can be found from a simple equilibrium condition of the normal forces in the direction of the applied load, as shown in Fig. 9. Hence, an estimate of the plastic zone at failure loads ($P^0 = P_{ul}$) can be given by:

$$R = \frac{cP_{ul}}{\tau^*} \quad [12]$$

Table 2 shows the corresponding predictions of the plastic zones R. Substitution of Eq 12 into Eq 11 yields:

$$P_{ul}/\left(1 - \frac{2c}{W}\right) + 2\tau^*/\pi(a_2 - a_1)\left[-a_1^2 \ln\left(\frac{1 + \sqrt{1 + a_1^2\beta^2}}{a_1\beta}\right) + a_2^2 \ln\left(\frac{1 + \sqrt{1 + a_2^2\beta^2}}{a_2\beta}\right)\right] - \sigma_{un} = 0 \quad [13]$$

where

$$\beta = \frac{cP_{ul}}{\bar{\omega}\tau^*}$$

The only unknown in Eq 13, which represents the final form of the strength prediction criterion, is the ultimate stress P_{ul}, which needs to be found by iterations. Clearly, for an unnotched specimen ($2c/W = 0$), Eq 13 reduces to the following:

$$P_{ul} = \sigma_{un}$$

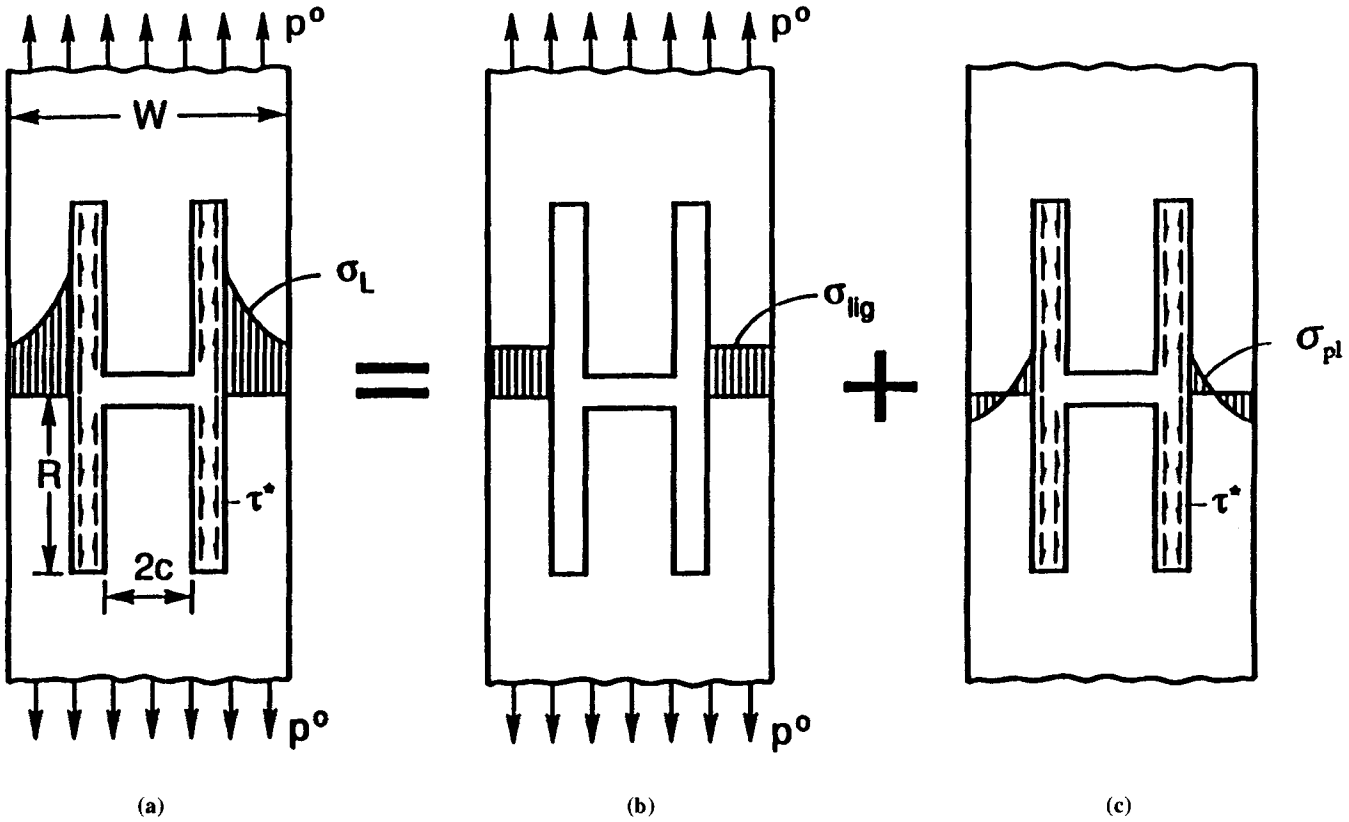

Fig. 6 Schematic decomposition of the normal local stress component, σ_L, into ligament stress, σ_{lig}, and plastic zone-induced stress, σ_{pl}.

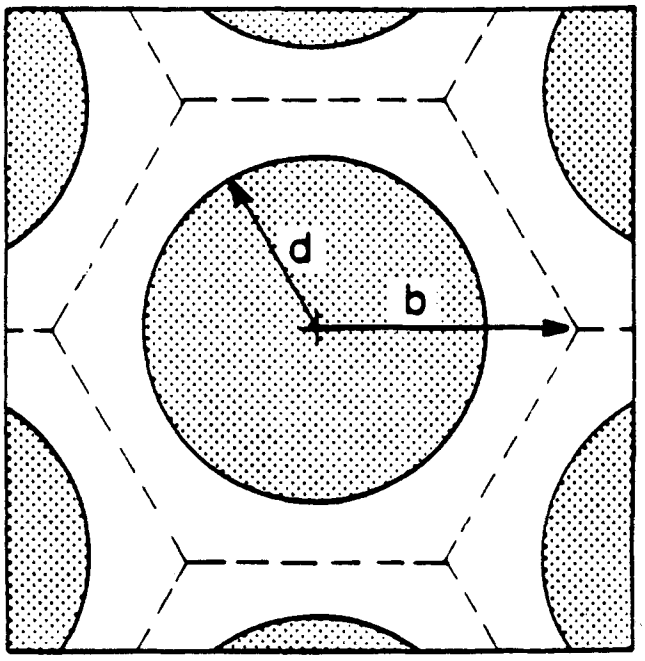

Fig. 7 Transverse plane geometry of a periodic fibrous composite.

which, in essence, is compatible with the model. Furthermore, it also includes all parameters involved in the fracture process.

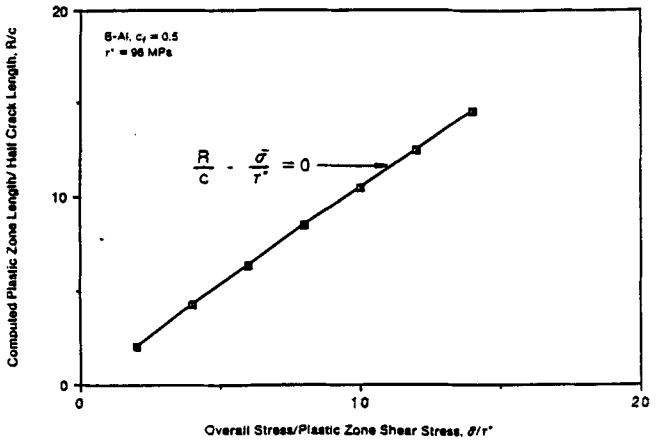

Fig. 8 Computed values of the plastic zone length to the half crack length ratio, R/c, in terms of the ultimate load to the composite flow stress ratio, P_{ul}/τ^*, at fracture loads.

4. Experimental Verification

The experimental justification of the model is examined here through comparison of current results with other experimental works. The first set of results is concerned with center-notched specimens of 6061 B/Al in the as-fabricated condition. As shown in Fig. 10, the fracture data for specimens of 1 in. width (25.4 mm) were obtained from the experimental work of

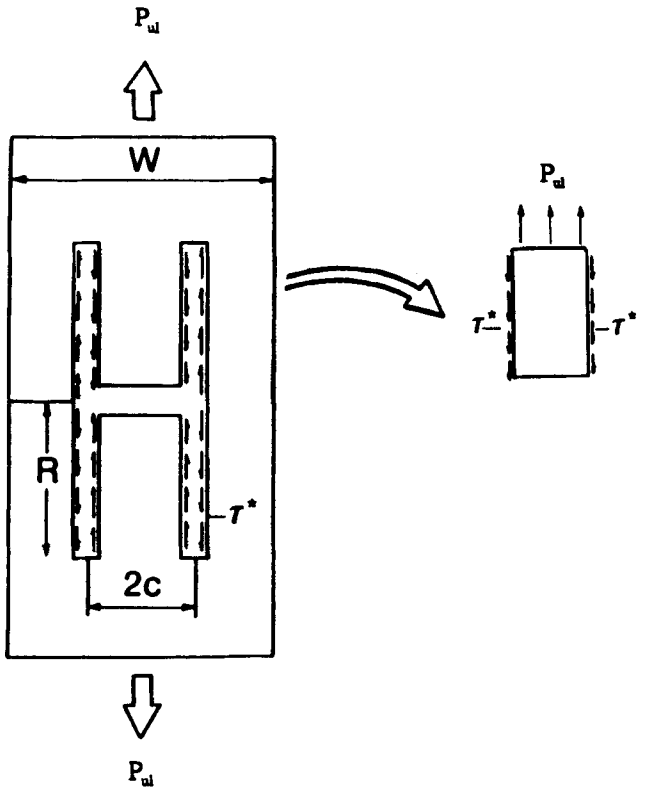

Fig. 9 Free-body diagram of the upper half of the *H*-crack configuration under uniform normal ultimate load.

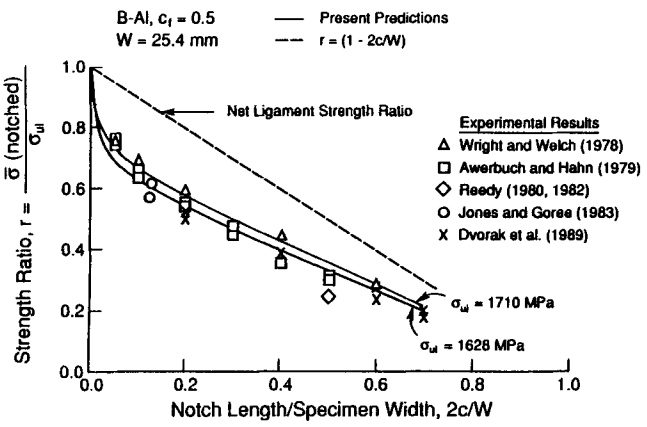

Fig. 10 Fracture strength reduction in 1-in.-wide center-notched B/Al specimens. Experimental data points are compared with the present predictions (solid lines).

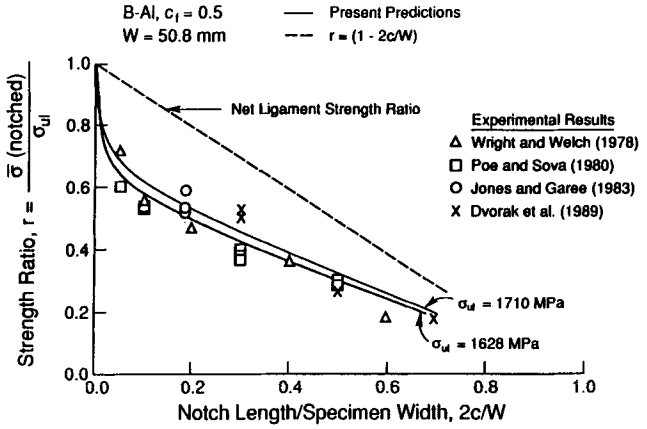

Fig. 11 Fracture strength reduction in 2-in.-wide center-notched B/Al specimens. Experimental data points are compared with the present predictions (solid lines).

Wright and Welch,[20] Poe and Sova,[4] Jones and Goree,[21] and Dvorak and Bahei-El-Din.[6] These data are plotted with symbols of different shapes, whereas the solid curve represents the prediction of the present model. Due to the scattered values of the unnotched strength obtained from different sets of experiments, the predicted results were based on two values of the unnotched strength: an upper value of 1710 MPa and a lower value of 1685 MPa. Therefore, the corresponding predictions were normalized by an upper and lower value of σ_{un}, respectively. Although the dashed line joining both ends of the curves describes the strength reduction contributed by the net ligament stress, the area between the straight dashed line and each curve denotes the strength reduction caused by the plastic zone. Also, Fig. 10 shows that for all $2c/W$ ratios, the experimental results agreed well with those determined by the present model.

Another set of results is shown in Fig. 11 for 2-in. (50.8-mm.) wide specimens of the same material. Again, the predicted results were in good agreement with most of the experimental data. Direct comparison of the results of the 1-in. specimens (Fig. 10) and 2-in. specimens (Fig. 11), indicates a slight shift in the predicted curves, which indicates a decrease in strength in the larger width specimens. Therefore, the width effect is clearly a factor in strength prediction. Other sets of results show the prediction of ultimate load to the composite flow stress ratio (P_{ul}/τ^*) for each of B/Al and FP/Al composite systems (Fig. 12 and 13). Although both composites exhibit a similar trend, the strength decrease in the FP/Al composite in terms of the $2c/W$ ratio is more pronounced.

5. Conclusion

The proposed model for strength prediction in fibrous metal matrix composites revealed that the fracture strengths of all examined specimens were controlled by an average local stress over a material representative volume element adjacent to the crack tip. The present model was proposed primarily to take into account the redistribution of local stress due to the plastic deformation at the crack tip. A Dugdale-type approach was then implemented to predict the length of these zones. In the process, the crack-interaction scheme proposed by Benveniste *et al.*[16] was used to numerically determine the stress-intensity factors in mode II for an *H*-crack in an infinite orthotropic material. The local normal stress was divided into two parts—a ligament stress, which is uniform over the uncracked ligament

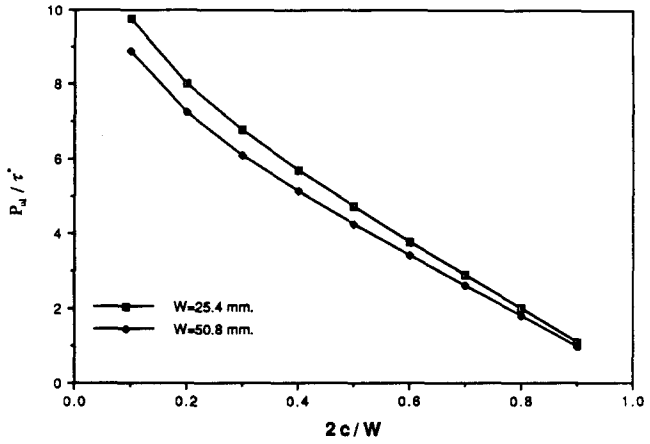

Fig. 12 Fracture strength reduction in 1- and 2-in.-wide center-notched B/Al specimens.

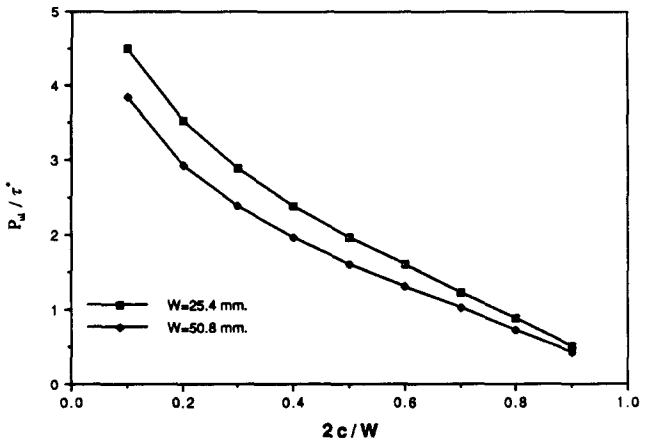

Fig. 13 Fracture strength reduction in 1- and 2-in.-wide center-notched FP/Al specimens.

of the specimen, and a plastic zone-induced stress, which has a zero average over the ligament. The latter was found to contribute 30 to 40% of the overall local stress field. The elastic solution of the otherwise discrete plastic zone was approximated by a single vertical crack of the same length and loaded by the flow stress of the composite material. The numerical results of this approximation correlate well with those found by experiment and by the finite-element method. Thus, a major simplification of the problem was obtained, because the fracture strength can now be predicted by a simple equation. The model is expected to be applicable to composites that exhibit similar localized plastic zones under uniform tensile loading condition. Finally, for future application, it is of interest to verify the possibility of expanding the current model to accommodate different crack orientations and applied loading conditions with respect to fiber direction. Other points of concern would be to characterize the limits of applicability of fracture variables. Such limits would certainly highlight the border of a small-scale yielding regime.

References

1. J. Awerbuch and H.T. Hahn, Crack-Tip Damage and Fracture Toughness of Boron/Aluminum Composites, *J. Comp. Mater.*, Vol 13, 1979, p 82-107.
2. E.D. Reedy, "On the Specimen Dependence of Unidirectional Boron/Aluminum Fracture Toughness," *J. Comp. Mater. Suppl.*, Vol 14, 1980, p 118-131.
3. E.D. Reedy, "Analysis of Center-Notched Monolayers with Application to Boron/Aluminum Composites," *J. Mechan. Phys. Solids*, Vol 28, 1980, p 265-286.
4. C.C. Poe and J.A. Sova,"Fracture Toughness of Boron/Aluminum Laminates With Various Proportions of 0° and ±45° Piles," NASA Technical Paper 1707, 1980.
5. G.J. Dvorak and Y.A. Bahei-El-Din, "Fracture of Fibrous Metal Matrix Composites, *Mechanics of Composite Materials*," Vol 92, G.J. Dvorak and N. Laws, Ed., ASME-AMD, New York, 1988, p 37-52.
6. G.J. Dvorak, Y.A. Bahei-El-Din, and L.C. Bank, "Fracture of Fibrous Metal Matrix Composites—I. Experimental Results," *Eng. Fract. Mechan.*, Vol 34, 1989, p 87-104.
7. J.R. Rice, "A Path Independent Integral and the Approximate Analysis of Strain Concentration by Notches and Cracks," *J. Appl. Mech.*, Vol 35, 1968, p 379-386.
8. F.A. McClintock, "Criterion for Ductile Fracture by the Growth of Holes," *J. Appl. Mech.*, Vol 35, 1968, p 363-371.
9. J. Tirosh, "The Effect of Plasticity and Crack Blunting on the Stress Distribution in Orthotropic Composite Materials," *J. Appl. Mechan.*, Vol 40, 1973, p 785.
10. Y.A. Bahei-El-Din, G.J. Dvorak, and J.F. Wu, "Fracture of Fibrous Metal Matrix Composites—II. Modeling and Numerical Analysis," *Eng. Fract. Mechan.*, Vol 34, 1989, p 105-123.
11. B.A. Bibly and K.H. Swinden, "Representation of Plasticity at Notches by Linear Dislocation Arrays," *Proc. Royal Soc., London*, Vol 285, 1965, p 22-33.
12. H. Riedel, "Plastic Yielding on Inclined Slip-Planes at a Crack Tip," *J. Mechan. Phys. Solids*, Vol 24, 1976, p 277.
13. V. Vitek, "Yielding on Inclined Planes at the Tip of a Crack Loaded in Uniform Tension," *J. Mechan. Phys. Solids*, Vol 24, 1976, p 265-275.
14. D. Kujawski and F. Ellyin, "On the Size of Plastic Zone Ahead of Crack Tip," *Eng. Fract. Mechan.*, Vol 25 (No. 2), 1986, p 229-236.
15. D.S. Dugdale, "Yielding of Steel Sheets Containing Slits," *J. Mechan. Phys. Solids*, Vol 8, 1960, p 100-104.
16. Y. Benveniste, G.J. Dvorak, J. Zarzour, and E.C.J. Wung, "On Interacting Cracks and Complex Crack Configurations in Linear Elastic Media," *Int. J. Solids Struct.*, Vol 25 (No. 11), 1989, p 1279-1293.
17. R.J. Nuismer and J.M. Whitney, "Uniaxial Failure of Composite Laminates Containing Stress Concentrations in Fracture Mechanics of Composites," STP 593, ASTM, 1972, p 299.
18. S.G. Lekhnitskii, "Theory of Elasticity on an Anisotropic Elastic Body," translated by P. Fern, Holden-Day, San Francisco, 1963.
19. N.I. Muskhelishvili, *Some Basic Problems of Mathematical Theory of Elasticity*, P. Noordhoff Groningen, The Netherlands, 1953.
20. M.A. Wright and D. Welch, "Failure of Centre Notched Specimens of 6061 Aluminum Reinforced With Unidirectional Boron Fibers," *Fibre Sci. Technol.*, Vol 11, 1978, p 447-461.

21. W.F. Jones and J.C. Goree, "Fracture Behavior of Unidirectional Boron/Aluminum Composite Laminates," *Mechanics of Composite Materials 1983*, Vol 58, G.J. Dvorak, Ed., ASME-AMD, 1983, p 171-177.

22. E.D. Reedy, "Notched Unidirectional Boron/Aluminum: Effect of Matrix Properties," *J. Compos. Mater.*, Vol 16, 1982, p 495-509.

23. E.D. Reedy, "Large Strain Shear Response of Unidirectional Boron/Aluminum," *Proc. Joint Jpn. Soc. Mechanical Engineers/Society for Experimental Stress Analysis Conference on Experimental Mechanics*, Hawaii, 22-23 May 1982, p 223-229.

24. N. Tsangarakis, J.M. Slepetz, and J. Nuneo, "Static and Fatigue Notch Strength Prediction in Alumina Fiber Reinforced Aluminum Plates with a Circular Hole," *J. Compos. Mater.*, Vol 22, 1988, p 386-393.

Appendix

In this Appendix, a derivation for the average value of the plastic zone-induced normal stress, σ_{pl}, over a representative volume element, $\bar{\omega}$, is performed. In the (x,y) coordinate system of Fig. 5, the average of σ_{pl} along the y-axis over a real segment $[t_1,t_2]$ can be written in the following general form:

$$\bar{\sigma}_{pl} = \frac{1}{(t_2 - t_1)} \int_{t_1}^{t_2} \sigma_{pl}(y)\,dy \qquad [A1]$$

Substitution of σ_{pl} from Eq 5 into Eq A1 provides an integrable function, which depends explicitly on y as:

$$\bar{\sigma}_{pl} / \tau^* = \frac{2}{\pi(t_2 - t_1)(a_2 - a_1)} \left[a_1^2 \int_{t_1}^{t_2} \frac{dy}{(1 + K_1^2 y^2)^{1/2}} - a_1^2 \int_{t_1}^{t_2} \ln(\alpha_1)\,dy - a_2^2 \int_{t_1}^{t_2} \frac{dy}{(1 + K_2^2 y^2)^{1/2}} - a_2^2 \int_{t_1}^{t_2} \ln(\alpha_2) \right] \qquad [A2]$$

where $K_{1,2} = a_{1,2}/R$ and

$$\alpha_{1,2} = \frac{1 + [1 + K_{1,2}^2 y^2]^{1/2}}{K_{1,2} y}$$

Evaluation of Eq A2 is somewhat cumbersome and necessitates integration by parts. Therefore, for the sake of simplicity, the following definitions are considered:

$$I_1 = \int_{t_1}^{t_2} \frac{dy}{(1 + K_1^2 y^2)^{1/2}}$$

$$I_2 = \int_{t_1}^{t_2} \ln(\alpha_1)\,dy$$

$$I_3 = \int_{t_1}^{t_2} \frac{dy}{(1 + K_2^2 y^2)^{1/2}}$$

$$I_4 = \int_{t_1}^{t_2} \ln(\alpha_2)\,dy \qquad [A3]$$

Hence, Eq A2 can be rewritten in the following way:

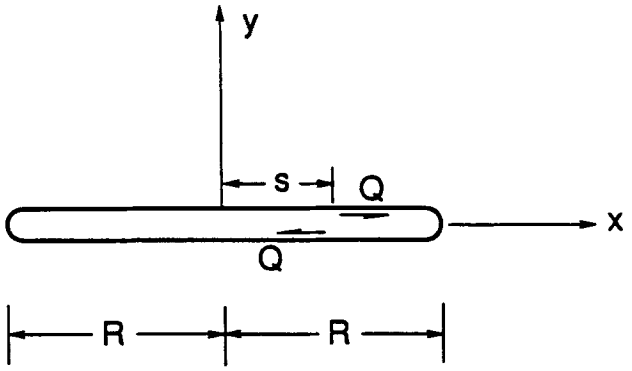

Fig. A-1 Geometry of a single crack loaded by concentrated shear loads.

$$\bar{\sigma}_{pl} / \tau^* = \frac{2}{\pi(t_2 - t_1)(a_2 - a_1)} \left[a_1^2 (I_1 - I_2) + a_2^2 (I_4 - I_3) \right] \qquad [A4]$$

In what follows, the integration of each part of Eq A3 will be considered separately. For instance, the evaluation of I_1 (or I_3) is first obtained by considering a change of variable, $K_1 y = t$, which yields the following:

$$I_1 = \frac{1}{K_1} \ln \left[\frac{K_1 t_2 + (1 + K_1^2 t_2^2)^{1/2}}{K_1 t_1 + (1 + K_1^2 t_1^2)^{1/2}} \right] \qquad [A5]$$

Similarly, I_3 is obtained from Eq A5 by simply replacing K_1 with K_2. A similar change of variable is made for I_2 (or I_4) and the final expression is:

$$I_2 = t_1 \ln(K_1 t_1) - t_2 \ln(K_1 t_2) + t_2 \ln \left[1 + (1 + K_1^2 t_2^2)^{1/2} \right] - t_1 \ln \left[1 + (1 + K_1^2 t_1^2)^{1/2} \right] - \frac{1}{K_1} \ln \left[\frac{K_1 t_1 + (1 + K_1^2 t_1^2)^{1/2}}{K_2 t_2 + (1 + K_1^2 t_2^2)^{1/2}} \right] \qquad [A6]$$

and I_4 is also obtained by substituting K_2 for K_1 in Eq A6. Finally, after assembling the above terms, one can write the overall expression for $\bar{\sigma}_{pl}$, normalized by the composite flow stress, τ^*, in the following way:

$$\bar{\sigma}_{pl}/\tau^* = \frac{2}{\pi(t_2 - t_1)(a_2 - a_1)} \left\{ -a_1^2 \left[t_1 \ln \left(\frac{K_1 t_1}{1 + (1 + K_1^2 t_1^2)^{1/2}} \right) + t_2 \ln \left(\frac{1 + (1 + K_1^2 t_1^2)^{1/2}}{K_1 t_2} \right) \right] + a_2^2 \left[t_1 \ln \left(\frac{K_2 t_1}{1 + (1 + K_2^2 t_1^2)^{1/2}} \right) + t_2 \ln \left(\frac{1 + (1 + K_2^2 t_2^2)^{1/2}}{K_2 t_2} \right) \right] \right\} \quad [A7]$$

The present goal is to average $\bar{\sigma}_{pl}$ over a representative volume element along the notch tip. Therefore, replacing t_2 with $\bar{\omega}$ in Eq A7 and taking the limit as the other variable t_1 goes to zero, provides the final expression of the average value of the plastic zone-induced normal stress as:

$$\bar{\sigma}_{pl}/\tau^* = \frac{2}{\pi(a_2 - a_1)} \left\{ -a_1^2 \ln \left[\frac{1 + (1 + (a_1/t)^2)^{1/2}}{(a_1/t)} \right] + a_2^2 \ln \left[\frac{1 + (1 + (a_2/t)^2)^{1/2}}{(a_2/t)} \right] \right\} \quad [A8]$$

where $t = R/\bar{\omega}$.

It can be shown that for large ratios, $R/\bar{\omega}$, in Eq A8, the rate of change in the slope of $\bar{\sigma}_{pl}/\tau^*$ is very slow, which suggests that with large plastic zone R, the induced normal stress over a representative volume element is contributed primarily by a certain length of the zone and certainly not the full zone length.